ChemComm

ROYAL SOCIETY OF CHEMISTRY

FEATURE ARTICLE

View Article Online
View Journal | View Issue

Cite this: *Chem. Commun.*, 2020, **56**, 10809

A review of recent work on using metal–organic frameworks to grow carbon nanotubes

Xian Wang,[a] Anrui Dong,[a] Yue Hu, *[a] Jinjie Qian *[a] and Shaoming Huang *[b]

Carbon nanotubes (CNTs) have long been known as a class of one-dimensional carbon nanomaterials with sp^2-hybridized structures that can be constructed with a very large length-to-diameter ratio, which is significantly larger than that of any other carbon nanomaterials. It is well known that CNTs exhibit many excellent properties in mechanics, electricity, chemistry, optics, *etc.*, and are widely used in various fields, thus attracting scientists' attention. In this context, the development of new strategies for optimizing and synthesizing CNTs has far-reaching significance and demand. On the other hand, most metal–organic frameworks (MOFs) are microporous crystals constructed from ordered and uniform metal ions/clusters and organic linkers to obtain crystalline solids with potential porosity. Using MOF materials as precursors, hierarchical CNT-based composite materials, which are difficult to synthesize through the traditional catalyst-assisted chemical vapor deposition method, can be conveniently synthesized by thermal treatment at high temperature. In the process of converting MOFs into CNTs, MOF crystals are used as both catalysts and carbon sources, which are necessary for the growth of CNTs, and they are also used as templates and/or carriers for additional catalysts. Therefore, there are various possibilities for the thermal conversion of MOFs into CNT-based composite materials. In this review, we mainly summarize the two aspects of catalysts and synthetic strategies for MOF-derived CNT-based composite materials. Despite the rapid development in this area, there is still much space for exploration. In order to accurately control the synthesis of CNTs, we should deeply explore the thermal conversion process and mechanism for the conversion of MOFs into CNTs.

Received 9th June 2020,
Accepted 3rd August 2020

DOI: 10.1039/d0cc04015k

rsc.li/chemcomm

1. Background

Carbon nanotubes (CNTs) have long been known in the form of multi-wall carbon nanotubes (MWCNTs) based on nested single-wall carbon nanotubes (SWCNTs), which are a class of one-dimensional nanomaterials with a radial dimension of

[a] *College of Chemistry and Materials Engineering, Wenzhou University, Wenzhou 325035, Zhejiang, China. E-mail: yuehu@wzu.edu.cn, jinjieqian@wzu.edu.cn*
[b] *School of Materials and Energy, Guangdong University of Technology, Guangzhou 510006, Guangdong, China. E-mail: smhuang@gdut.edu.cn*

Xian Wang

Xian Wang received his bachelor degree from Shenyang University of Chemical Technology, China. He is now an MS student at the College of Chemistry and Materials Engineering, Wenzhou University. His current research is focused on the design and growth of MOF single crystals, converting MOFs into different types of carbon materials by heat treatment, and analyzing the structure and electrochemical properties of the derived materials.

Anrui Dong

Anrui Dong is an undergraduate student at Wenzhou University. His current research is mainly focused on the synthesis of MOFs and derived carbon materials for electrocatalysis and metal–air batteries.

nanometers and an axial dimension of micrometers.[1] Such tube-based structures were first observed by Radushkevich and Lukyanovich in 1952.[2] Subsequently, a Japanese scientist, Dr Iijima of the NEC Corporation, described CNTs in detail in *Nature* in 1991,[3] which ignited extensive research by scientists.[4] It is well known that the carbon element in CNTs exhibits sp^2 hybridization,[5] and CNTs are endowed with many excellent mechanical,[6,7] electrical,[8,9] chemical,[10] optical[11,12] and thermal properties.[13] In this context, CNT-based composites made from two or more constituent materials, which have significantly different physicochemical properties when combined with CNTs, can be widely used in various applications, such as electrocatalysis,[14,15] nanoelectronic devices,[16,17] thermally conductive films,[18] structural materials for aviation,[19] *etc.* Among the facile synthetic methods,[4] catalyst-assisted chemical vapor deposition (CCVD)[20] can efficiently control the growth of various desired SWCNTs as well as MWCNTs and is utilized on a large scale. To date, optimizing and developing new strategies for growing CNTs still has far-reaching significance and necessity.[21]

Yue Hu

Dr Yue Hu is an Associate Professor in the College of Chemistry and Materials Engineering, Wenzhou University. He received his PhD degree from Peking University under the supervision of CAS Academician Jin Zhang. His current research focuses on the preparation of single-walled carbon nanotubes by structural control, the investigation of their conductive properties, and related electronic devices.

On the other hand, metal–organic frameworks (MOFs) are ordered and porous crystalline materials built from metal ions/clusters and organic ligands through versatile coordination bonds.[22] According to reported research, the combination of MOFs and CNTs could enhance the electrochemical energy storage and conversion[23,24] and catalytic performance[25] of their composite materials. Therefore, researchers have considered the *in situ* conversion of MOFs into MOF-derived CNT-based composites,[26] which is a convenient strategy for improving the properties of these derived materials.[27,28] In recent years, due to MOFs' unique pore structures and controllable morphology, and the combination of metal components and carbon sources,[29] people have been keen to use MOF precursors for designing and synthesizing various metal-based and carbon-based nanocomposite materials by pyrolysis at high temperature.[30] Many previous studies have shown that by adjusting the pyrolytic conditions and the combination of ligands and metal species in the MOF materials, the structure and morphology of the derived carbon materials can be controlled and tuned,[31] thereby preparing a variety of carbon materials, such as graphitized carbon nanosheets,[32,33] carbon nanotubes,[34,35] porous carbon,[36,37] *etc.* At present, due to technical reasons, there are no literature reports on MOF-derived SWCNTs, which need to be explored in the future, so we only discuss MOF-derived MWCNTs in the following. In 2013, Yang *et al.* doped ZIF-8 with iron ions and pyrolyzed a mixture of the resulting Zn-Fe-ZIF crystals and dicyandiamide under a nitrogen atmosphere, so that N-doped CNT-based composites (NCNTs) were first obtained from a MOF template,[38] which has drawn people's attention to the strategy of converting MOFs into CNTs.

In the transformation process, MOFs can simultaneously act as both catalysts and carbon sources, which are vital for the growth of CNTs,[39–41] as well as templates and carriers for additional catalysts and carbon sources,[42–44] providing unlimited possibilities for achieving the thermal conversion

Jinjie Qian

Dr Jinjie Qian received his PhD degree from Fujian Institute of Research on the Structure of Matter, Chinese Academy of Sciences, under the supervision of CAS Academician Maochun Hong. He is an Associate Professor in the College of Chemistry and Materials Engineering, Wenzhou University. His current research involves electrochemical research on nanostructures with adjustable morphology and derivatives of metal–organic frameworks for energy storage and conversion.

Shaoming Huang

Dr Shaoming Huang is a professor in the School of Materials and Energy, Guangdong University of Technology. He received his PhD from Nankai University in 1991. From 1996 to 2005, he worked at the University of Sussex in the UK, the Commonwealth Institute of Science and Industry (CSIRO), and Duke University in the USA. Over the past decade, his group has devoted itself to basic research and related application technology development of micro–nano structural–functional materials, including carbon nanostructured materials (especially carbon nanotubes), metal nanomaterials, and inorganic functional materials.

of crystalline MOFs to synthesize CNT-based nanocomposite materials.[45] In addition, due to the spatial confinement effect and the energy released during the breakage of coordination bonds,[46] the pyrolysis of MOF materials helps to activate metal-based catalyst nanoparticles (NPs) and organic components and provides favorable conditions for the reorganization of carbon species to form CNTs.[47] Furthermore, the morphologies of MOFs are diverse and easy to control,[48,49] and this can be exploited to prepare the expected hierarchical CNT-based structures and composites,[50,51] which are difficult to obtain through traditional CCVD methods. With the emerging prospects of MOF-derived CNT-based nanomaterials in energy-related applications, herein we mainly summarize MOF-derived CNT-based composite materials from the perspective of catalysts and synthetic strategies as listed in Table 1. Finally, recent challenges will be discussed and future perspectives will be proposed for designing and preparing more promising MOF-derived CNT-based nanomaterials for wide ranging applications in various fields.

2. Catalysts for CNT growth

Generally speaking, high catalytic activity catalysts play a key role in the growth of CNTs.[52,53] Although CNTs can grow without the presence of catalysts,[54] the efficient growth of CNTs heavily relies on the participation of catalysts.[55] Traditionally, according to vapor–liquid–solid theory,[56] iron group transition metal NPs such as iron,[57] cobalt,[58] and nickel[59] are widely used to catalyze the formation of CNTs. Among them, polymetallic alloys like FeNi,[60] CoNi,[61] FeNiCo,[62] *etc.* also exhibit highly efficient catalytic activity to construct CNTs. Different metals have different interactions with carbon and show different carbon solubility, so the carbon layer is etched by dissolving carbon or

Table 1 A summary of MOF-derived CNT-based materials

	Composition of MOF		External components					
Material	Metal	Ligand	Metal species	Carbon sources	Substrate	Calcination conditions	Catalyst	Ref.
NCNTs	Zn	2-Methylimidazole	$FeSO_4$	Dicyandiamide	n.a.	N_2, 900 °C	Fe/Fe_3C	38
N-CNT-assembled dodecahedra	Co	2-Methylimidazole	n.a.	n.a.	n.a.	Ar, 435 °C	Co	47
N-CNT-assembled microspheres	Ni	2-Methylimidazole	n.a.	n.a.	n.a.	Ar, 435 °C	Ni	
N-CNT-assembled microspheres	Ni	Trimesic acid	n.a.	n.a.	n.a.	Ar, 435 °C	Ni	
CNT-assembled microsheets	Co	Trimesic acid	n.a.	n.a.	n.a.	Ar, 430 °C	Co	
CNT-assembled hollow microspheres	Co	Terephthalic acid	n.a.	n.a.	n.a.	Ar, 430 °C	Co	
MIL/CNT–Fe	Fe	2-Aminoterephthalic acid	n.a.	n.a.	n.a.	N_2, 800 °C	Fe	74
Co/NCNHP	Zn, Co	2-Methylimidazole	n.a.	n.a.	n.a.	Ar, 900 °C	Co	40
MIL-88-Fe/Ni	Fe, Ni	Terephthalic acid	n.a.	Dicyandiamide	n.a.	Ar, 800 °C	$FeNi_3$	75
(Fe,Co)/CNT	Zn, Co	2-Methylimidazole	$FeCl_3$	n.a.	n.a.	N_2, 900 °C	FeCo	76
NiCo/NCNTs	Co, Ni	2-Methylimidazole	n.a.	n.a.	n.a.	Ar/H_2 (9/1), 700 °C	NiCo	77
Fe_3Mn_1/N-CNTs-100	Mn	2,5-Dihydroxylbenzoic acid	$Fe(NO_3)_3$	n.a.	n.a.	N_2, 800 °C	FeMn	78
CoO-NCNTs	Co	3,4,5,6-Tetrahydrophthalate, 1,4-diazabicyclo[2.2.2]octane	n.a.	n.a.	n.a.	Ar/H_2 (9/1), 800 °C	CoO	85
Fe/Fe_3C@NGL-NCNT	Fe	Terephthalic acid	n.a.	n.a.	n.a.	N_2, 700 °C	Fe/Fe_3C	86
NCNTFs	Co	2-Methylimidazole	n.a.	n.a.	n.a.	Ar/H_2 (9/1), 700 °C	Co	101
Co@N-CNTs@rGO	Zn, Co	2-Methylimidazole	n.a.	n.a.	Reduced graphene oxide	Ar, 900 °C	Co	102
Co_9S_8@CT	Zr	Terephthalic acid	$CoCl_2$	Thiourea	n.a.	N_2, 800 °C	Co_9S_8	95
Fe–N-CNTs-H	Zn	2-Methylimidazole	$FeC_6H_5O_7$	n.a.	n.a.	Ar, 950 °C	Fe	106
3D-CNTA	Co	2-Methylimidazole	n.a.	Melamine	n.a.	N_2, 650 °C	Co	111
MSZIF-T	Co	2-Methylimidazole	n.a.	n.a.	Melamine sponge	N_2, 900 °C	Co	112
NCo@CNT-NF	Co	2,5-Dihydroxyterephthalic acid	n.a.	Dicyandiamide	n.a.	Ar, 700 °C	Co	113
CoCHs-3	Co	2-Methylimidazole	n.a.	Melamine	Polyacrylonitrile film	N_2, 700 °C	Co	122
Ni@CNTs	Ni	Terephthalic acid	n.a.	n.a.	Ni foam	N_2/H_2 (95/5), 600 °C	Ni	123
CoInNC@CNT	Co, In	2-Methylimidazole, biphenyl-3,3′,5,5′-tetracarboxylic acid	n.a.	Dicyandiamide	InOF-1 rod	$Ar/H_2/C_2H_2$ (10/10/0.55), 800 °C	$Co_3InC_{0.75}$	115
FeCo/FeCo-Ni@NCNTs-HF	Fe, Co	Potassium hexacyanoferrate	$Ni(NO_3)_2$	Melamine	Polyacrylonitrile film	1. Ar, 550 °C; 2. N_2, 800 °C	FeCoNi	126
NGPC/NCNTs	Zn	Terephthalic acid	Nickel formate	Urea	n.a.	1. N_2, 550 °C; 2. N_2, 800 °C	Ni	127

by catalytic carbon hydrogenation at a high temperature. Fe, Co, *etc.* have a large carbon solubility, while Au, Cu, *etc.* have a low carbon solubility.[63] The dissolution and precipitation of carbon by metal particles may lead to reorganization of the carbon structure and the formation of defective carbon, core–shell structures of carbon-encapsulated metal particles, *etc.*[64] Besides, some literature has reported that metallic compounds such as ZrO_2/HfO_2[65] and TiO_2[66] can also catalyze CNT growth, which confirms that catalysts with only nanoscale curvature and carbon adsorption sites can also diffuse carbon segments on the crystal planes,[67] so that CNTs can efficiently grow along the specific crystal lattice.[52] Using particulate catalysts, the CCVD growth method is popular for the preparation of CNT materials, as it yields high-quality nanotubes and exhibits a degree of control over diameter, length, and morphology, but achieving repeatability is a major problem.[21] In this context, porous coordination polymers are structurally composed of metal and carbon species, thus pristine MOF materials can be intrinsically and steadily self-catalyzed by MOF-derived metal-based catalysts to construct CNTs according to the previously reported literature.[68] Furthermore, introducing external catalysts into the large pores and channels of MOFs and replacing the original coordinating nodes through transmetallation and impregnation are two common and reliable approaches for the uniform distribution of introduced metal atoms in MOF structures (Fig. 1). We can choose to introduce[46] or not introduce additional catalysts[69] into the MOF precursors which will be decomposed and reduced to form different types of metal-based particulate catalysts (single metals, polymetallic alloys, metallic compounds, *etc.*) under the high-temperature pyrolysis conditions. In summary, in the pyrolysis process, there are three different types of catalysts which can efficiently catalyze and grow CNTs. In this section, we are going to divide the MOF-derived catalysts for CNT growth into the following types for discussion: (1) single metal catalysts, (2) polymetallic alloy catalysts, and (3) metallic compound catalysts. They grow CNTs through two different catalytic mechanisms. Single metals, polymetallic alloys, and metal carbides with carbon solubility grow CNTs according to the vapor–liquid–solid theory.[70] Metallic compounds composed of metals and nonmetals (excluding metal carbides) provide only nanoscale curvature and carbon adsorption sites for diffusing carbon segments on the crystal planes so that CNTs can efficiently grow along the specific crystal lattice.[65]

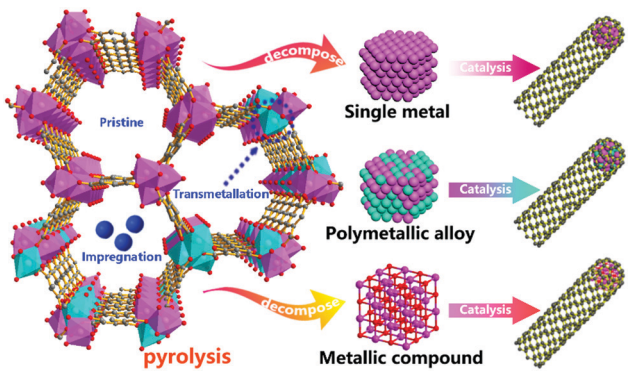

Fig. 1 Schematic diagram of the formation of MOF-derived CNTs catalyzed by three types of catalysts, namely single metals, polymetallic alloys, and metallic compounds.

2.1 Single metal catalysts

As always, metal elements have been considered to be the best catalysts and many researchers have found that single metal NPs (like Fe,[71] Co,[72] Ni[73]) can efficiently catalyze the formation of CNTs through calcination of the corresponding MOFs. In 2017, Mai's group developed a simple, versatile, and efficient strategy to pyrolyze MOF crystals in which a single MOF precursor with its own nanocatalyst and carbon sources is decomposed *in situ* to form a CNT composite with the same morphology by pyrolysis at 435 °C under argon.[47] A schematic diagram of the transformation of a ZIF-67 crystal into a hollow CNT-assembled dodecahedron is shown in Fig. 2a, where the ZIF-67 dodecahedron is pyrolyzed under the protection of Ar at a low temperature. The coordination bond between the metal ion and the organic ligand in ZIF-67 is first broken and the overall structure is gradually decomposed, while the metal ions/clusters are further reduced to nanocatalysts by the generated reductive gas, and these *in situ* formed nanocatalysts catalyze the formation of N-doped CNTs (N-CNTs) from the residual organic ligands. Since metal nanocrystals preferentially form on the surface, the outer layer is first converted into N-CNTs, and the growth direction is from outside to inside, resulting in internal voids. In Fig. 2b, the thin multi-walled N-CNTs are abundant (10–20 nm outer diameter and 5 nm inner diameter), and the cobalt NP (5 nm diameter) catalysts are encapsulated at the tips of the CNTs. On the one hand, it is found that nanocatalysts derived from iron group based MOFs exhibit high catalytic activity for the *in situ* formation of CNTs. Secondly, organic ligands with abundant hexatomic or N-heterocyclic carbon rings can lower the cyclization energy barrier and promote the formation of CNTs. Moreover, the decomposed coordination bonds in highly ordered MOFs release more energy to activate the remaining metal ions/clusters as well as organic linkers, thereby facilitating the formation of nanocatalysts and the following growth of CNTs. On the other hand, the particle size of the catalyst has a huge influence on the growth process of CNTs, and a smaller catalyst is more beneficial to the growth of CNTs. Therefore, it is vital to control the pyrolytic conditions to obtain abundant nanocatalysts. Additionally, this method can be successfully extended to other iron group based MOFs, including Ni-ZIF, Ni-BTC, Co-BTC, Co-MOF, *etc.*, to obtain the corresponding MOF-derived CNT assembly architectures (Fig. 2c–f). Zhu *et al.* also reported for the first time that a new N-molecule-assisted autocatalytic carbonization process converts iron-based MIL-88B-NH_2 into conductive CNTs and micro/mesoporous carbon composites (MIL/CNT-Fe).[74] During the calcination process, the volatile ammonia gas reduces the Fe element in the Fe-MOF to iron nanocrystals, which catalyze the formation of Fe,N-doped CNTs, while the remaining framework is etched by ammonia gas to obtain a type of micro/mesoporous carbon structure (Fig. 2g). In general, by selecting single metal catalysts with

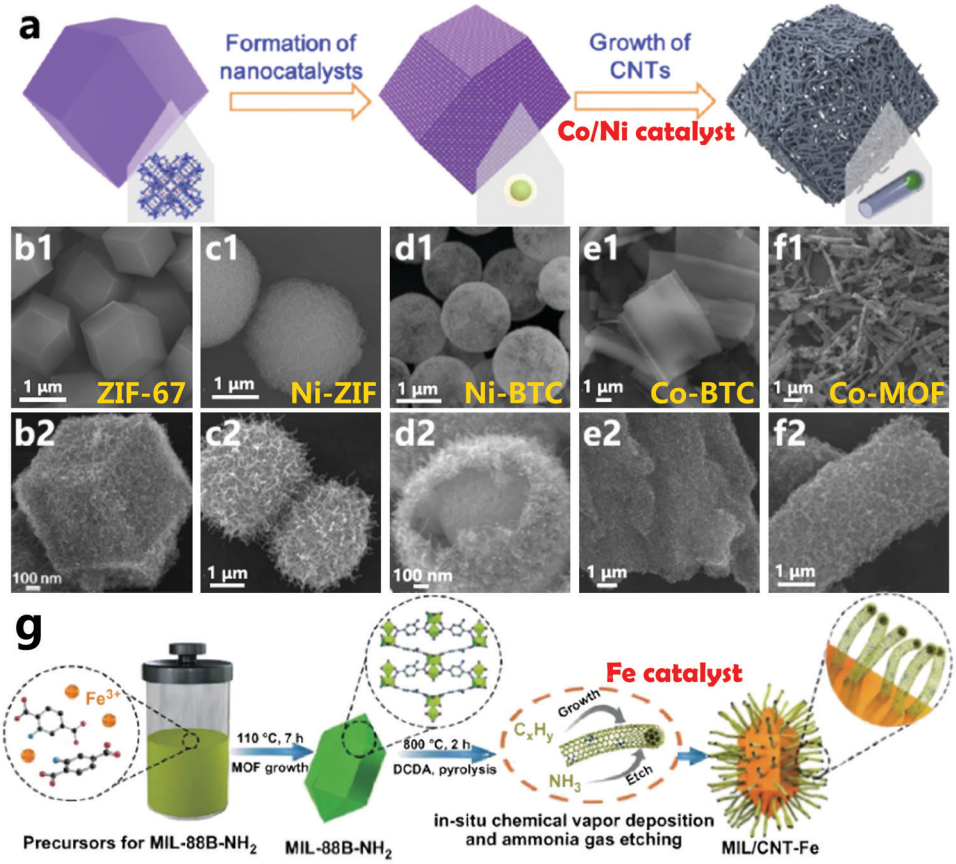

Fig. 2 (a) Schematic of the formation process of N-CNTs from ZIF-67, finally obtaining an N-CNT-assembled hollow dodecahedron. (b1 and b2) SEM images of the ZIF-67 precursor and the derived N-CNT-assembled hollow dodecahedron; (c1 and c2) SEM images of the Ni-ZIF precursor and the derived N-CNT-assembled microspheres; (d1 and d2) SEM images of the Ni-BTC precursor and the derived CNT-assembled hollow microspheres; (e1 and e2) SEM images of the Co-BTC precursor and the derived CNT-assembled microsheets; (f1 and f2) SEM images of the Co-MOF precursor and the derived CNT-assembled nanorods. Reprinted with permission from ref. 47. Copyright (2017) American Chemical Society. (g) Illustrative procedure for the iron(III)-2-aminoterephthalic framework (MIL-88B-NH_2, MIL = Materials from the Lavoisier Institute) and the resultant CNT and Fe-decorated carbon hybrids (MIL/CNT-Fe). Reprinted with permission from ref. 74. Copyright (2019) Springer Nature.

high carbon solubility, especially iron group metals, CNT-based composites can be easily synthesized from the corresponding MOFs. We believe that by controlling the pyrolytic conditions, this single metal catalyst strategy can be further extended to other metals (Cu,[79] Au,[80] W,[81] Mo,[82] *etc.*), which are considered to have low carbon solubility, for the *in situ* growth of MOF-derived CNT composites with adjustable components and morphology.

2.2 Polymetallic alloy catalysts

In principle, metal alloys can also catalyze the assembly of carbon sources into CNTs.[83] Arne Thomas *et al.* reported the preparation of bifunctional catalysts (FeNi catalysts) *via* one-step pyrolysis of a mixture of bimetallic MIL-88-Fe/Ni and dicyandiamide (DCDA) to obtain MOF-derived N-doped carbon materials (Fe–Ni@NC-CNTs).[75] First, by a solvothermal method, terephthalic acid, $FeCl_3$ salt, and $Ni(NO_3)_2$ salt were assembled into MIL-88-Fe/Ni nanorods. After that, DCDA and the crystalline MOF precursor were physically mixed by mechanical grinding, and pyrolyzed in an inert atmosphere at 800 °C (Fig. 3a). The TEM image of Fe–Ni@NC-CNTs clearly demonstrated that a uniform and porous CNT-anchored network was observed (Fig. 3b), and the nanorod morphology of the precursor could be partially retained. High-resolution TEM showed a particle at the tip of the derived CNT, which was attributed to $FeNi_3$ NPs, which confirmed that the formation of CNTs was conveniently catalyzed by the FeNi alloy (Fig. 3c). In 2018, Wu and colleagues introduced Fe^{3+} cations into a Zn/Co bimetallic organic framework, denoted by Zn_1Co_1-BMOF, and the formed Fe–Co dual sites were annealed at 900 °C in an N_2 atmosphere to catalyze the decomposition of the organic ligands in the bimetallic MOF precursor, thus FeCo alloy NPs embedded in N-doped CNTs [(Fe,Co)/CNT] which were rich in Fe–Co dual sites were successfully constructed (Fig. 3d and e).[76] The Fe and Co atoms were coordinated with N at the atomic scale, which was confirmed by the EEL spectrum (Fig. 3f). And bimetallic NiCo-ZIF is a suitable precursor for the growth of NiCo/NCNTs as shown in Fig. 3g.[77] It is easily reduced into NiCo NPs and almost completely converted into CNTs after being annealed at 700 °C under an H_2/Ar atmosphere. Zhang *et al.* prepared a

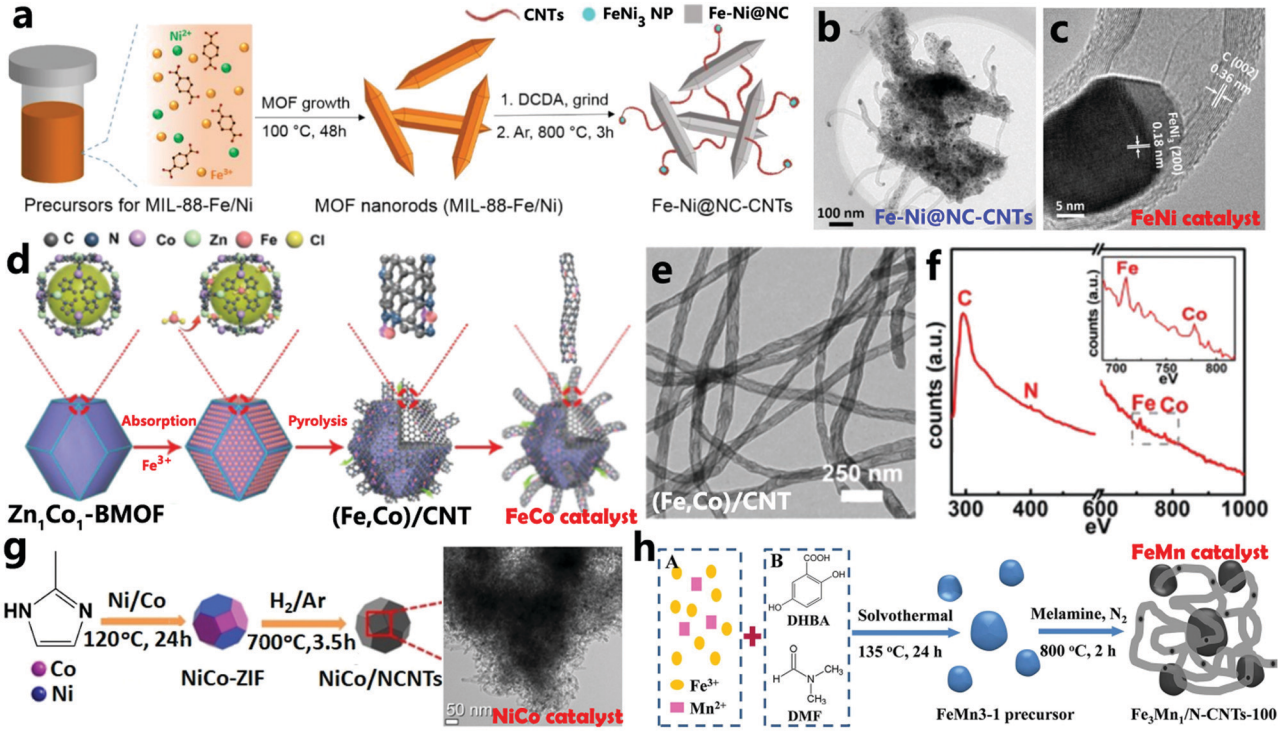

Fig. 3 (a) Synthetic procedure of MIL-88-Fe/Ni and Fe–Ni@NC-CNTs, (b and c) TEM images of Fe–Ni@NC-CNTs. Reprinted with permission from ref. 75. Copyright (2018) Wiley. (d) Schematic image of the preparation of (Fe,Co)/CNT, (e) TEM image, and (f) the EEL spectrum of (Fe,Co)/CNT. Reprinted with permission from ref. 76. Copyright (2018) Royal Society of Chemistry. (g) Scheme of the synthesis of NiCo/NCNTs. Reprinted with permission from ref. 77. Copyright (2020) Elsevier. (h) Illustration of the preparation of the FeMn3-1 precursor and the derived Fe_3Mn_1/N-CNTs-100 catalyst. Reprinted with permission from ref. 78. Copyright (2018) Wiley.

bimetallic FeMn3-1 template which was subsequently treated by thermal carbonization with melamine. They successfully obtained a hierarchical carbon structure of Fe_3Mn_1 alloy NPs coated with N-doped CNTs (Fe_3Mn_1/N-CNTs-100) (Fig. 3h),[78] in which Fe may be beneficial to the formation of a carbon layer on the surface of the NPs, and Mn can promote the growth and elongation of CNTs. The synergistic effects of different metals in the polymetallic alloy help to regulate the shape and quality of the obtained carbon materials.[55,84] Thus, we believe that polymetallic alloys consisting of iron group metals (Fe, Co, Ni) and other metals with high carbon solubility are likely to have high catalytic activity for the formation of CNTs,[52] and reconstituted polymetallic alloy catalysts of various types are conducive to the development of different CNT-based nanocomposites for further applications.

2.3 Metallic compound catalysts

Compared with pure metals, metal oxides are thought to have low catalytic activity for growing CNTs.[87] Different from the vapor–liquid–solid theory, CNTs can grow on metal oxides based on the intragranular charge transfer transition and the lattice strain of the catalyst NPs.[52] In 2019, Ding *et al.* reported a two-dimensional network of nitrogen-doped CNTs derived from a porous pillar-layered coordination polymer (1Co)[85] with a two-dimensional sheet morphology as shown in Fig. 4a and b. After pyrolysis of the lamellar MOF, a two-dimensional network constructed from NCNTs, denoted by CoO-NCNTs, is formed, catalyzed by CoO NPs (Fig. 4c and d). According to the HRTEM image in Fig. 4e, cobalt oxide particles are wrapped and held at the tips of the CNTs, and the CNT (002) and CoO (111) lattice planes are clearly observed, verifying that the formation of the CNTs is catalyzed by the CoO NPs. The distribution of elements can be seen more clearly from the EDX mapping of a single nanotube, and the main diffraction peaks completely coincide with those of cubic CoO (JCPDS #78-0431), indicating the presence of CoO NPs (Fig. 4f). Furthermore, the carbon and nitrogen elements are evenly distributed around the entire nanotube, while cobalt and oxygen are only localized at the tip of a single CNT (Fig. 4g–i). Many studies have confirmed that iron carbide could be an efficient catalyst for the growth of CNTs. Ya-Qian Lan's group was the first one to report the successful synthesis of a novel N-doped Fe/Fe_3C-graphitized layer/carbon nanotube complex (Fe/Fe_3C@NGL-NCNT) by one step *in situ* pyrolysis using MIL-101(Fe) as a solid precursor (Fig. 4j).[86] As shown by HRTEM (Fig. 4k), these Fe_3C NPs are fully coated with a 5 nm thick graphitic carbon layer, and the lattice spacing of 0.24 nm is reasonably assigned to the (210) crystal plane of Fe_3C. During the process of MOF pyrolysis, the energy released by the bond breaking provides favorable conditions[47] for the *in situ* synthesis of CNTs catalyzed by metallic compounds, which can form unique nanocomposites combined with metallic compounds and CNTs that cannot be synthesized by conventional methods. In the field of using metallic compounds to grow CNTs, there is still a lot of space for us to explore whether nitrides,[88] sulfides,[89] phosphides,[31]

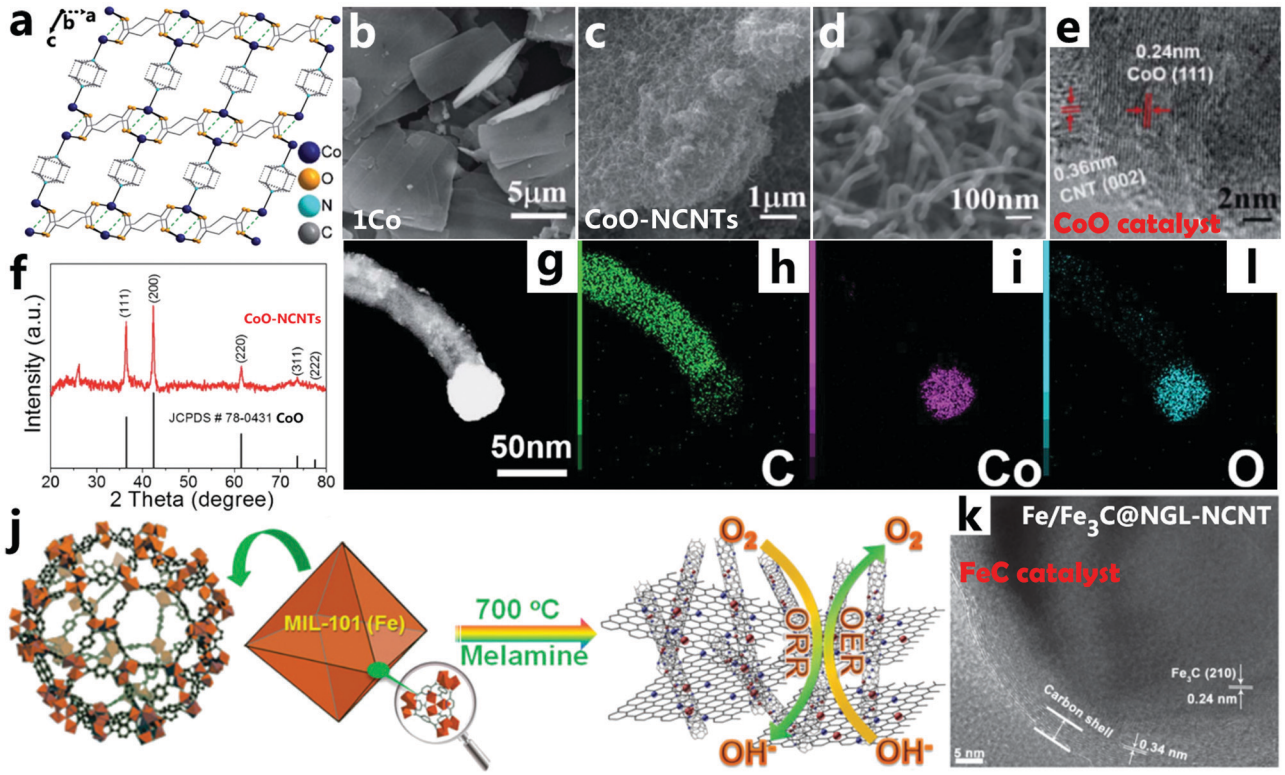

Fig. 4 (a) The coordination environment of 1Co. The single layers of 1Co are parallel to the *ac* plane, and the layers are stacked along the *b* axis. (b) SEM image of 1Co, (c and d) SEM, and (e) HRTEM images of CoO-NCNTs. (f) PXRD pattern of as-made CoO-NCNTs. (g–l) Elemental mapping of a single nanotube of CoO-NCNTs. Reprinted with permission from ref. 85. Copyright (2019) Royal Society of Chemistry. (j) The synthetic procedure of Fe/Fe_3C@NGL-NCNT as a bifunctional electrocatalyst: blue balls – nitrogen atoms, brown balls – Fe/Fe_3C species. (k) HRTEM image of Fe/Fe_3C@NGL-NCNT. Reprinted with permission from ref. 86. Copyright (2015) Royal Society of Chemistry.

selenides,[90] *etc.* have the potential to catalyze the formation of CNTs and their composites through MOF pyrolysis.

3. Synthetic strategy

Since 2013, researchers have been dedicated to the development of various strategies for designing and synthesizing MOF-derived CNT-based composites for energy-related applications.[91] During pyrolysis, the coordination bonds break and the pristine MOFs are decomposed into metal or metallic compound NPs and some active organic species can be formed *in situ*.[47] This process usually involves high energy (500–1000 °C) to atomize the resulting reactive gaseous carbon sources that diffuse toward the catalyst-coated substrate and condense to form CNTs. Generally speaking, it is possible to prepare CNTs through the coexistence of catalysts with high catalytic activity and sufficient carbon sources under suitable pyrolytic conditions.[92] To explain the general mechanism of the growth of CNTs, first of all, the metal atoms, which are either already present in the MOF or introduced, are aggregated at high temperature to form thermodynamically stable catalyst nanoparticles. Then, carbon sources derived from the ligands of the MOF or external carbon sources are thermally decomposed to form carbon species which adsorb on the surface of the catalyst nanoparticles. Finally, with the help of catalysts, CNTs are finally formed.[52] In this section, we are going to introduce five different strategies for the synthesis of MOF-derived CNT-based composites by pyrolysis with the assistance of catalysts (Fig. 5), and discuss several typical examples that have been studied to fully demonstrate that MOF precursors can be converted into CNT-based nanomaterials through versatile approaches. First, precursors like ZIF-67[93] contain the Co element, which can be transformed into highly active catalyst NPs, and the heterocyclic 2-MeIm ligand with a low cyclization energy barrier. Therefore, in the pyrolysis process, the ligands act as the carbon source. Secondly, in ZIF-8,[94] UiO-66,[95] *etc.*, the metals provided by the MOFs themselves either cannot catalyze the decomposition of the carbon source to synthesize carbon tubes or exhibit poor catalytic activity. Thus, we can introduce external metals (Fe,[96] Co,[97] Ni,[98] Cu,[99] Mo,[100] *etc.*) with high catalytic activity into these systems by transmetallation and/or impregnation, in order to catalyze the decomposition of the carbon components in the MOFs to form CNTs. Third, some ligands have high cyclization energy barriers and/or lower carbon content, and the ligand content in the MOF materials is also limited. Thus, in order to obtain high yield and high-quality CNTs, we need to add some additional carbon sources, such as dicyandiamide, melamine, ethylene, acetylene, *etc.*[69] Fourth, to obtain hierarchical MOF-derived CNT-based composites with the

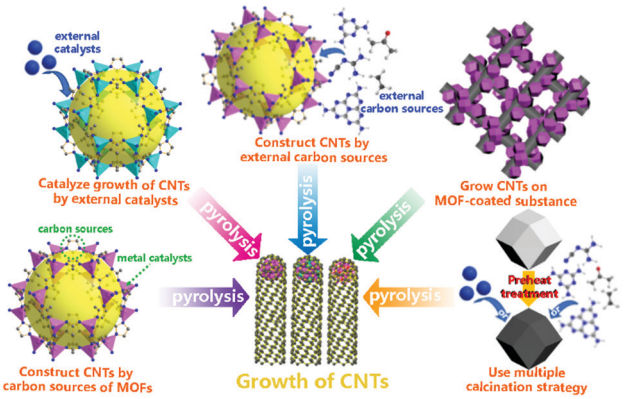

Fig. 5 Schematic of five different synthetic strategies for growing MOF-derived CNT-based nanomaterials.

beneficial properties of a substrate,[103] we can first combine the MOF with the substrate, and then achieve the three-dimensional substrate coated with CNTs by pyrolysis. Finally, through the strategy of multiple calcination, the introduction of additional carbon sources and/or catalysts during the calcination of the pre-carbonized material can change the surface morphology and carbon layer structure of the material to generate CNTs by a stepwise approach.[104]

3.1 Constructing CNTs with carbon sources from MOFs

MOF structures constructed from metal atoms with high catalytic activity for the direct growth of CNTs and organic ligands rich in carbon rings easily form CNT-based materials under certain conditions.[40,105] In 2016, Lou *et al.* reported the research work of a hollow N-doped carbon nanotube frameworks (NCNTFs) derived from ZIF-67 polyhedra. Interestingly, ZIF-67 particles would provide both carbon source and catalyst for the syntheses of CNTs, and serve as the template for the formation of hollow skeletons.[101] In Fig. 6a and b, the SEM images exhibit uniform NCNTFs assembled by interconnected CNTs obtained after thermal treatment at 700 °C, where the shape of the precursor is well preserved. Then we learn that the as-obtained NCNTFs possess a layered shell of interconnected N-doped CNTs with a thickness of 200 nm, and the TEM image confirms its hollow structure which stems from the volatilization of organic linkers and the consumption of growing CNTs (Fig. 6c). Furthermore, HRTEM images also revealed the presence of Co NPs, which are encased at the tips of the CNTs as expected (Fig. 6d). In this case, H_2 flow is the key to generating the hierarchical CNT framework with a hollow morphology. As the carbon source is provided by ZIF-67 itself, a large number of cobalt NPs are rapidly formed in the H_2 atmosphere, and then the outer carbon is preferentially converted into CNTs, finally leading to hollow NCNTFs, while the ZIF-67 template does not form CNTs on being annealed at 600 and 900 °C in the absence of H_2 (Fig. 6g and h). Moreover, in the hydrogen atmosphere, as the target temperature increases, the thermal decomposition will be more complete, and in this way longer and denser CNTs are more easily formed at 900 °C in comparison with the product formed at 600 °C (Fig. 6e and f). Fang *et al.* developed a new and effective method to synthesize ultrafine Co NPs encapsulated in nitrogen-doped carbon nanotubes (N-CNTs) grafted onto both sides of reduced graphene oxide (rGO) (Co@N-CNTs@rGO) through direct annealing of graphene oxide loaded with core–shell bimetallic ZIF particles (Fig. 6i).[102] First, ZIF-8 nanocrystals are easily grown on both sides of the graphene oxide (GO) sheet to give ZIF-8@GO as a substrate (Fig. 6j). Subsequently, ZIF-67 crystals are epitaxially grown on the ZIF-8 seeds to form a sandwich-like structure (ZIF-67@ZIF-8@GO) which is embedded with core–shell crystals. Finally, reduction and carbonization of the ZIF-67@ZIF-8@GO precursor is thermally induced at 900 °C to obtain the Co@N-CNTs@rGO hybrid composite with a three-dimensional hierarchical structure. Due to the catalytic effect of Co species, the organic ligands in the core–shell ZIF-67@ZIF-8 crystals are totally converted into N-CNTs with a Co NP core and N-CNT shell at high temperature. In Fig. 6k, abundant CNTs are distributed on the surface of rGO, in which the *in situ* generated N-CNTs are not severely aggregated and are seamlessly integrated with the rGO sheet. In this type of core–shell ZIF-67@ZIF-8 crystals, the cobalt ions are present in an appropriate quantity with uniform distribution so that they do not easily aggregate into large cobalt particles with low catalytic activity, and the zinc ions volatilize, leading to the formation of pores at the same time, which is more conducive to catalyzing the growth of CNTs from a carbon source obtained from the MOF. Using the ligand units of MOFs as the carbon source for growing CNTs has the following advantages: (1) the activated organic ligands formed from the broken coordination bonds during pyrolysis are conducive to further reaction to form CNTs; (2) the presence of hexatomic or N-heterocyclic carbon rings can efficiently lower the cyclization energy barrier during the process of CNT formation; (3) the uniform distribution of metal atoms and ligands inhibits aggregation of the catalysts and facilitates full contact between the carbon source and the catalysts for efficient growth of CNTs. It is worth noting that in the presence of limited organic components, excess amounts of metal species in MOFs would lead to the formation of large catalyst particles which would severely hamper efficient CNT production.[51]

3.2 Catalysis of the growth of CNTs by external catalysts

During CNT precipitation, carbon vapors tend to cool down rapidly during expansion, and carbon atoms would quickly condense to form tubular structures with the help of specific catalyst particles.[107] However, the metals in some MOFs sometimes do not exhibit efficient catalytic activity for growing CNTs, so approaches for the *ex situ* introduction of other highly active catalysts, including transmetallation and impregnation, can also be used to generate CNTs.[44] The research group of Tian encapsulated Co ions and thiourea (Thu) molecules in the amino-decorated Zr-based MOF UiO-66-NH_2, and successfully obtained a novel earthworm-like N,S-doped carbon nanotube-encapsulated Co_9S_8 hybrid (Co_9S_8@CT) by one-step calcination (Fig. 7a).[95] The two immiscible phases consist of a mixture of

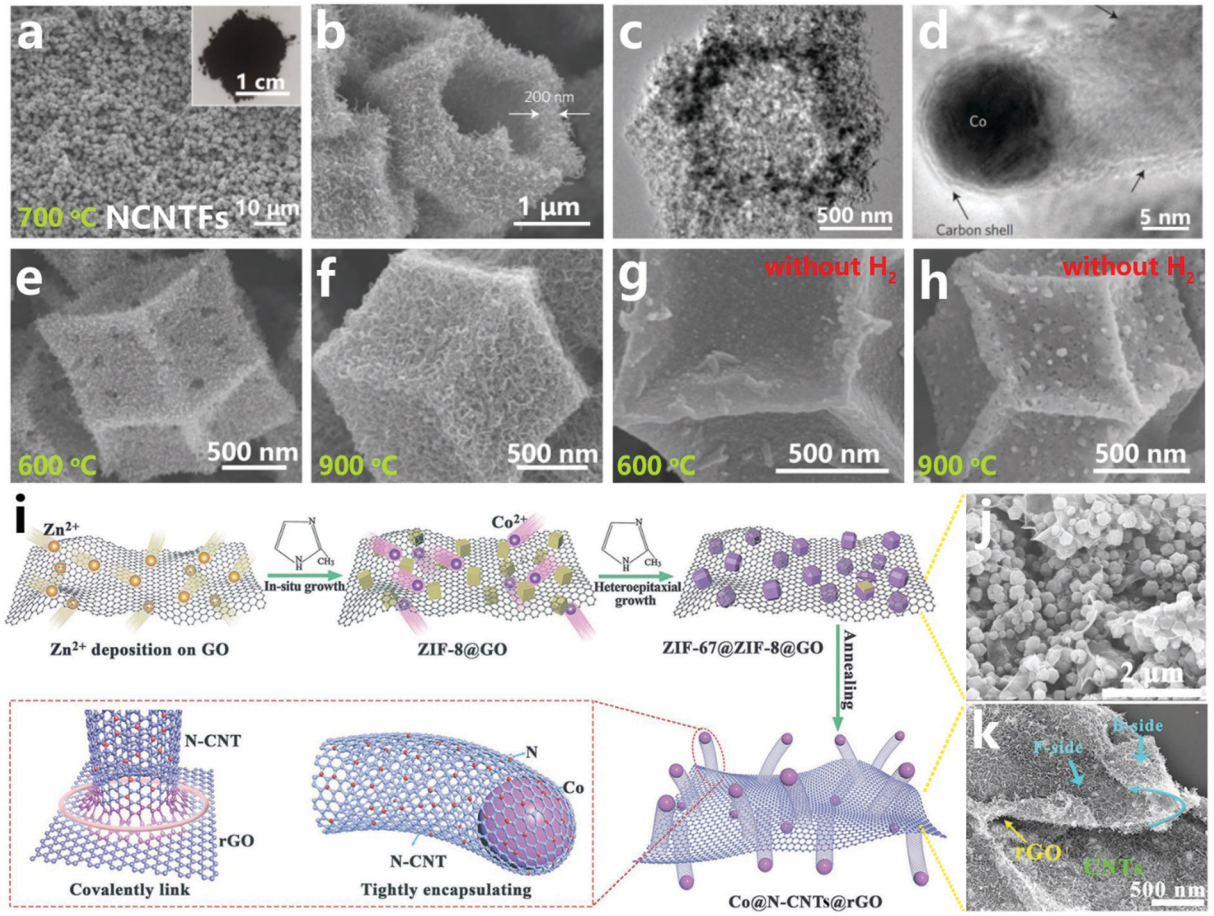

Fig. 6 (a and b) SEM, (c) TEM, and (d) HRTEM images of NCNTFs obtained at 700 °C in the presence of H_2. SEM images of ZIF-67 heat-treated at 600 °C (e) and 900 °C (f) in the presence of H_2, and heat-treated at 600 °C (g) and 900 °C (h) in the absence of H_2. Reprinted with permission from ref. 101. Copyright (2016) Springer Nature. (i) Synthetic preparation of Co@N-CNTs@rGO hybrid composites, (j) SEM image of the ZIF-67@ZIF-8@GO composite, and (k) SEM image of Co@N-CNTs@rGO. Reprinted with permission from ref. 102. Copyright (2018) Wiley.

$UiO\text{-}66\text{-}NH_2$ crystals dispersed in hydrophobic hexane solvent and a hydrophilic methanol–water mixture containing the Thu and $CoCl_2$ guest molecules. During agitation, the hydrophilic pore environment of $UiO\text{-}66\text{-}NH_2$ induces thiourea and $CoCl_2$ to enter the microsized cavity, thus a Co(II) + Thu@$UiO\text{-}66\text{-}NH_2$ complex that encapsulates Thu and $CoCl_2$ molecules is steadily constructed. Within the limited space of the $UiO\text{-}66\text{-}NH_2$ pores, the close contact between the guest molecules and the MOF is further strengthened, and the generated Co species are used to catalyze the formation of CNTs. In a second example, Wei's group directly pyrolyzed ferric salt-impregnated MOFs to synthesize Fe and N-doped CNTs. As shown in Fig. 7b, ZIF-8 is structurally made up of zinc atoms, which makes it difficult to grow CNTs by simple pyrolysis due to zinc vaporization at high temperature.[106] Compared with the Fe–N-CNTs obtained with ferric chloride (Fig. 7c and d), the carbon tubes of Fe–N-CNTs-H obtained by introducing iron citrate show a larger diameter of >0.1 μm. Due to the strong interaction between citrate and metal ions, citric acid molecules can partially replace the 2-methylimidazole ligands, while the Zn nodes in ZIF-8 are partially substituted with Fe and the overall coordination structure is not completely destroyed or decomposed. This newly formed composite can induce the transformation of iron citrate into larger Fe NPs during pyrolysis, thus constructing CNTs with a large diameter. Plenty of metals are thought to show catalytic activity to assemble carbon species into CNTs, like Ni,[108] Mo,[82] W,[81] Au,[80] *etc.* Meanwhile, we can introduce metal salts,[45] polyoxometalates,[109] metal complexes,[33] organometallic compounds,[110] *etc.* which can be converted into effective and uniform nanocatalyst particles in the pyrolytic process. Using different catalysts can definitely tune the structure and morphology of the carbon materials and generate CNT-based composite materials with different functions for practical applications.

3.3 Constructing CNTs with external carbon sources

The CCVD method is the most promising way to produce CNTs on a large scale and utilizes high temperatures to atomize carbon sources, such as methanol, ethanol, methane, ethylene, carbon monoxide, and acetylene.[13] However, the limited content of organic components in pristine MOFs is not conducive to the preparation of high-yield CNTs,[114] so the introduction of external carbon sources would be beneficial to increasing the yield of CNTs. In this context, the Cao group has developed an

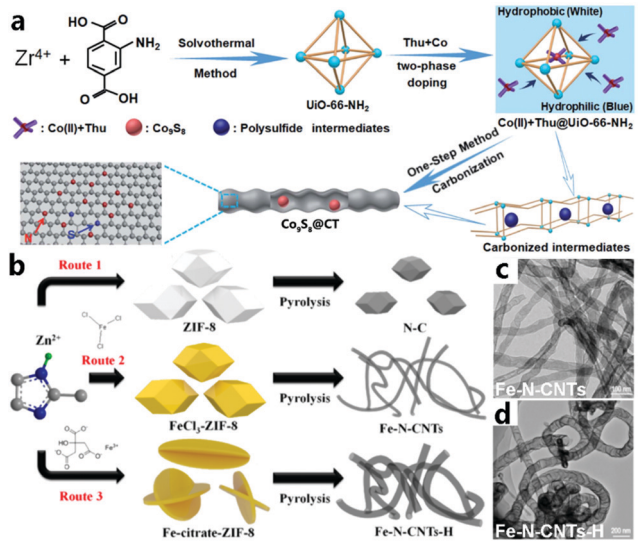

Fig. 7 (a) Schematic of the two-phase synthesis of CNT-encapsulated Co_9S_8 nanocomposites. Reprinted with permission from ref. 95. Copyright (2018) Royal Society of Chemistry. (b) Synthetic procedure of N–C, Fe–N-CNTs, and Fe–N-CNTs-H; (c and d) SEM images of Fe–N-CNTs and Fe–N-CNTs-H, respectively. Reprinted with permission from ref. 106. Copyright (2019) American Chemical Society.

efficient and low-cost MOF-induced strategy to synthesize a three-dimensional actiniae-like carbon nanotube assembly (3D-CNTA), where ZIF-67 is used as a precursor and mixed with a certain amount of melamine, and a two-step temperature-programmed pyrolysis process is conducted (Fig. 8a).[111] First, the furnace is set to 550 °C under an N_2 atmosphere so that g-C_3N_4 is efficiently polymerized by melamine, which uniformly penetrates the carbonized ZIF-67 polyhedra. Then, the target temperature is further increased up to 650 °C to cause g-C_3N_4 to decompose and release a large amount of carbonaceous gas, which is used as the carbon source for *in situ* orientated CNT growth. The as-obtained actiniae-like 3D-CNTA consists of nanospheres with an average size of 10 μm which are composed of many high-density CNTs (Fig. 8b). Interestingly, these CNTs gather toward the center of each sphere, which exhibits a zero-dimensional synaptic structure with Co NPs as the core and N-doped carbon layers as the shell (Fig. 8c). The formation of g-C_3N_4 plays an important role in the construction of CNTs, while simply mixing the MOF samples with melamine cannot produce 3D-CNTA with assembled nanotubes; instead, disordered nanotubes are formed following calcination. This indicates that the precursor of the carbon source has a great influence on the morphology and microstructure of the intermediate product. In 2017, Zhaosheng Li and colleagues proposed a method of simply loading a ZIF-67 film on a three-dimensional macroporous polymer substrate (melamine sponge), and further thermal decomposition produced a hierarchical three-dimensional nanocarbon structure (MSZIF-T).[112] The MSZIF-900 product is well characterized by dense CNTs growing vertically on three-dimensional macroporous carbon foam (Fig. 8d). Here, the melamine sponge not only serves as a three-dimensional macroporous supporting template, but also provides a suitable carbon source for the generation of CNTs at high temperature. As shown in Fig. 8e, Xu *et al.* successfully synthesized the first super-long single-crystal cobalt–organic framework (Co-MOF-NT) nanotubes with a diameter of approximately 70 nm and a length of 20–35 μm by controlling the recrystallization of amorphous Co-MOF-NP.[113] Subsequently, using dicyandiamide (DCDA) as both the nitrogen and carbon source, Co-MOF-NT and DCDA are annealed simultaneously to prepare a hierarchical structure (NCo@CNT-NF) composed of carbon nanofibers coated with abundant nitrogen-doped CNTs (20–30 nm in diameter and 200–300 nm in length). To sum up, the introduction of the external carbon source can increase the yield of CNTs. Moreover, there are many carbon sources to choose from, like ethylene,[115,116] dicyandiamide,[75] melamine,[103] C_3N_4,[117] thiourea,[118] *etc.*, to adjust the structure of the resulting CNTs. Heteroatomic carbon sources are beneficial for the formation of heteroatom-doped CNTs. Similarly, CNTs made from molecules that are rich in six-membered carbon rings have fewer defects than those made from five-membered or seven-membered carbon rings.[119] These defects and the presence of heteroatomic doping alter the original electronic structure of the CNTs, resulting in a complete change in the resulting electrochemical properties.[76]

3.4 Growing CNTs on MOF-coated substances

MOF-derived carbon material based electrodes for electrochemical reactions inevitably involve a casting solution of the active material, the conducting material and the polymer binder as well as the solvent, which will induce large interfacial impedance and reduce the electrode performance.[120] By using MOFs grown on the conductive substrate to produce the corresponding derivatives, hierarchical composite materials can be easily obtained which improves the corresponding properties.[121] In 2019, Huang *et al.* designed a stereoselective and autocatalytic assembly method to synthesize a series of carbon hybrids with a three-dimensional network structure (Fig. 9a).[122] In this strategy, a fiber film composed of polyacrylonitrile (PAN) nanofibers as a starting template is first prepared by electrospinning. Then, cobalt ions are electrostatically and preferentially adsorbed on the PAN fibers and assembled into a MOF-based film by facile coordination with 2-methylimidazole to obtain M@PAN fibers. Finally, the M@PAN fibers are annealed with melamine simultaneously at high temperature to form a hierarchical carbon fiber network modified by multi-walled carbon nanotubes (CoCHs). In this pyrolysis process, the PAN-derived carbon fibers can effectively protect the structural integrity, inhibit irregular catalyst aggregation, and make sure that the carbon hybrid material CoCHs exhibits a three-dimensional porous, flexible and stretchable nanostructure. Furthermore, a series of CoCHs precursors with different Co-MOF loading can be easily prepared by simply tuning the MOF nucleation time to 1 h, 2 h, 3 h, and 4 h. Among them, after the precursor with the highest MOF loading undergoes catalytic pyrolysis, the derived CoCH-4 shows abundant tangled CNTs. As shown in Fig. 9b, Peng *et al.* synthesized a vertical nanosized array of crystalline Ni-BDC on a nickel foam substrate (NF@Ni(BDC)) by a hydrothermal method, followed by

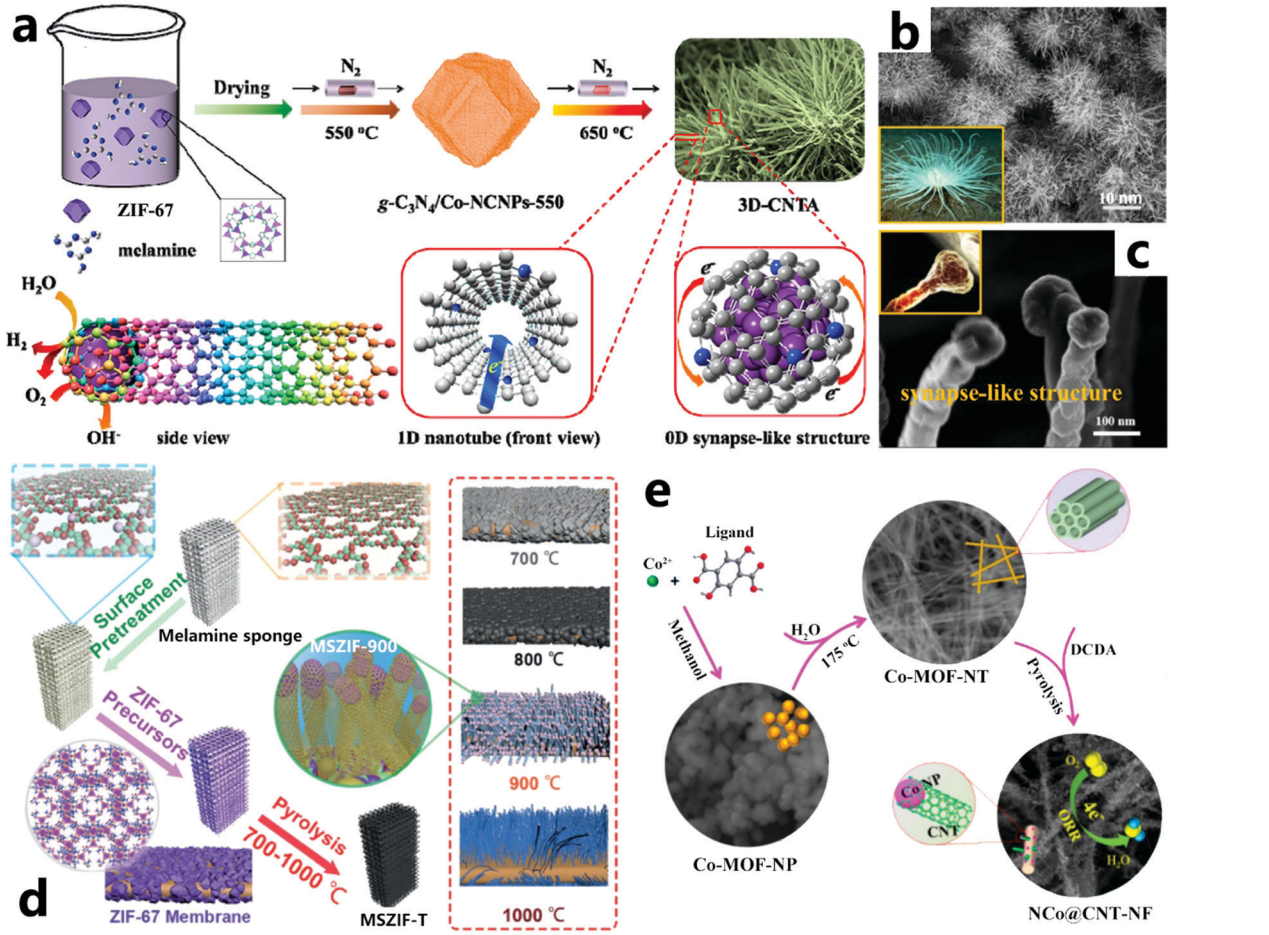

Fig. 8 (a) The fabrication process of 3D-CNTA, (b and c) SEM images of 3D-CNTA at different magnifications (the insets are digital photographs of an actiniae and a synapse, respectively). Reprinted with permission from ref. 111. Copyright (2017) Elsevier. (d) Illustration of the synthetic procedure for the MSZIF-T electrocatalysts. Reprinted with permission from ref. 112. Copyright (2017) Wiley. (e) Schematic diagram of the preparation of hierarchical carbon dendrites of NCo@CNT-NF. Reprinted with permission from ref. 113. Copyright (2018) American Chemical Society.

pyrolysis in H_2/N_2 mixed gas, in which a hierarchical structure of three-dimensional nickel foam wrapped in thin two-dimensional MOF-derived carbon nanosheets (Ni/C nanosheets) was successfully obtained. Interestingly, the nickel NPs in these thin MOF-derived carbon nanosheets are encapsulated in a few graphitized carbon layers or CNTs (Ni@CNTs), and exhibit superior electrocatalytic properties.[123] In 2020, our group designed a strategy for growing ZIF-67 polyhedra on an indium–organic framework (InOF-1) to prepare carbon rods coated with nitrogen-doped carbon nanotubes (CoInNC@CNT), as shown in Fig. 9c.[115] At first, through a solvothermal reaction, uniform rod-shaped nanocrystals of InOF-1 can be steadily obtained, and can be used as an excellent nano-substrate to support the ZIF-67 polyhedra to facilely produce the InOF-1@ZIF-67 precursor. According to the SEM images, the InOF-1 rod has a diameter of 200 nm and a smooth surface; the InOF-1@ZIF-67 composite shows a core–shell morphology where the ZIF-67 crystals are evenly distributed around the InOF-1 nanorods. After the *in situ* pyrolysis of InOF-1@ZIF-67 at 800 °C in $Ar/H_2/C_2H_4$ mixed gas, the CoInNC@CNT sample is conveniently obtained, and a large number of CNTs are grown on the surface of the carbonized InOF-1 rod. The catalytic growth of CNTs on the substrate inhibits the aggregation of catalysts as well as CNTs, and the derived materials can acquire the properties of the substrate like porosity,[112] conductivity,[51] flexibility,[124] *etc.* Possession of these useful properties broadens the application of MOF-derived materials in different fields.

3.5 Using multiple calcination strategies

MOF materials are structurally composed of inorganic metals and organic species together with various guest solvents as well as charge-balancing groups in their pore environment,[125] which means that it is sometimes difficult to directly grow CNTs from MOFs after heat treatment to form a complicated system. With multiple calcining processes, we can make up for the lack of precursor samples by adding external carbon sources and/or high activity catalysts to stimulate the formation of CNTs. In 2020, Lu and collaborators reported a two-step calcination to prepare FeCo/FeCoNi alloy NP-decorated N-doped CNT-grafted porous carbon fibers (FeCo/FeCoNi@NCNTs-HF), as shown in Fig. 10a.[126] On dispersing Prussian blue analogue KFeCo nanocubes into a solution of PAN, Ni ions and DMF, KFeCo/Ni^{2+}@PAN fibers are

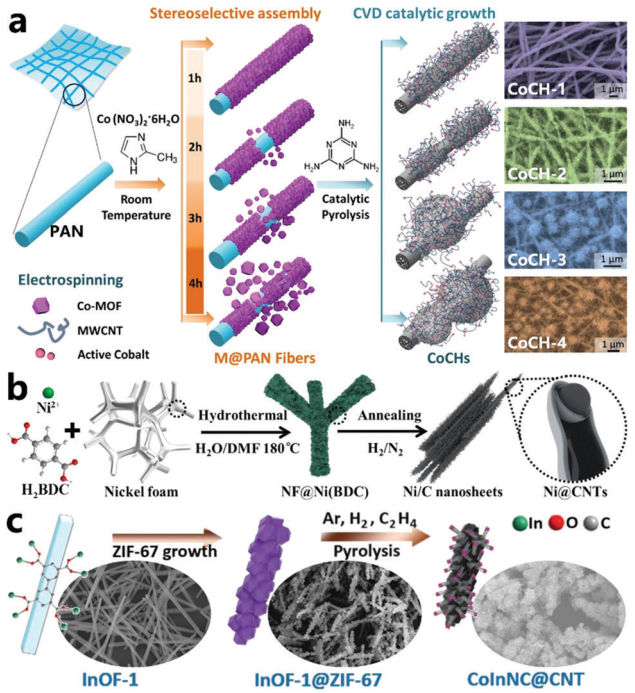

Fig. 9 (a) The synthesis of hierarchical CoCHs derived from M@PAN fibers, and SEM images of Co embedded hierarchical carbon hybrids: CoCH-1 (purple), CoCH-2 (green), CoCH-3 (blue), and CoCH-4 (orange) corresponding to the scheme of CoCHs with varying microstructures. Reprinted with permission from ref. 122. Copyright (2019) Wiley. (b) Schematic illustration of the preparation process of NF@Ni/C composites from the NF@Ni(BDC) precursor. Reprinted with permission from ref. 123. Copyright (2018) Royal Society of Chemistry. (c) Schematic illustration of the synthetic process for CoInNC@CNT composites. Reprinted with permission from ref. 115. Copyright (2020) Wiley.

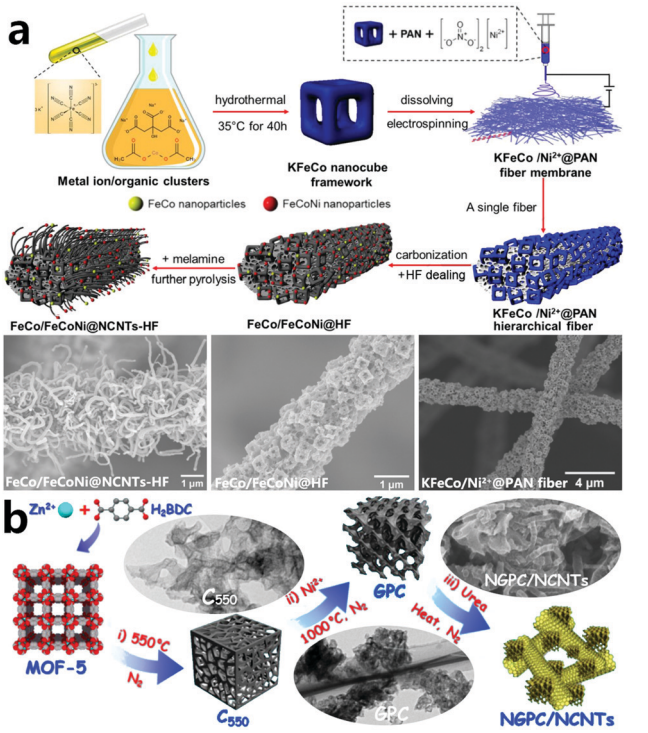

Fig. 10 (a) Schematic diagram of the preparation process for the FeCo/FeCoNi@NCNTs-HF membrane and its morphology, and the corresponding SEM images of KFeCo/Ni^{2+}@PAN hybrid fibers, FeCo/FeCoNi@HF, and FeCo/FeCoNi@NCNTs-HF. Reprinted with permission from ref. 126. Copyright (2019) Elsevier. (b) Illustration of the stepwise structural evolution from MOF-5 to NGPC/NCNTs. Reprinted with permission from ref. 127. Copyright (2015) American Chemical Society.

facilely produced by electrospinning in which KFeCo nanocubes are uniformly attached to the PAN fiber. After the first calcination at 900 °C in Ar, the morphology of the precursor is well maintained, and FeCo and FeCoNi alloy NPs are evenly dispersed throughout the porous fiber. Through HF etching, the obtained FeCo/FeCoNi@HF is reheated together with melamine. Because the tiny FeCo and FeCoNi alloy NPs still possess high activity for dissolving carbon and decomposing carbon sources, the hierarchical porous FeCo/FeCoNi@NCNTs-HF composite is eventually constructed. Similarly, Wang *et al.* developed a step-by-step method to synthesize nitrogen-doped graphitic porous carbon and carbon nanotubes (NGPC/NCNTs) by using both MOF-5 and urea as carbon–nitrogen precursors, and nickel metal as the graphitization catalyst (Fig. 10b).[127] In this work, MOF-5 crystals are preliminarily carbonized at 550 °C to obtain amorphous carbon denoted by C_{550}. Then, on adding the external catalyst of Ni ions, heating at 1000 °C, and acid treatment, highly graphitized porous carbon (GPC) is produced. In the final step of carbonization, urea is further added as an external carbon–nitrogen source to construct N-doped CNTs. The pre-carbonization conditions for MOF materials are relatively mild, which prevents violent etching of the carbon species by the decomposition gas and complete collapse of the MOF, and so the derived skeleton partially retains its morphology and can be used as a template for the subsequent reaction.[104] The pre-carbonized carbon material inherits the porous characteristics of the MOF, and facilitates the uniform distribution of the introduced catalyst, which behaves as a template for the final product. By multiple calcining processes, the surface of the pre-carbonized carbon material can be modified and the structure of the original carbon layer can be changed, which is a very effective post-processing method to obtain CNT-based composite materials.

4. Conclusions and perspectives

In the past few years, researchers have developed diverse strategies to easily and efficiently prepare unique MOF-derived CNT-based composite materials. Focusing on catalysts and synthetic strategies, we have reviewed the current research results and revealed the conditions and advantages of using MOF precursors to grow CNTs. First, MOF materials are regarded as good self-catalytic precursors containing both metal and carbon sources. Secondly, the abundant and large pore structures in MOFs are able to load external catalysts, and allow spatial confinement during calcination. Finally, the synthesis of MOFs is convenient and controllable, and MOFs can be easily loaded on other substrates or used to form precursors of hierarchical CNT-based composite materials *via*

the self-template method. Despite the recent rapid development of research in this area, there are still many deficiencies and much space to explore. (i) The specific process and mechanism of the catalysis of the formation of carbon components are not clear. (ii) The purity, uniformity, and structure of MOF-derived CNTs cannot yet be accurately controlled. (iii) The research on the direct growth of CNTs using metallic compounds is still inadequate. (iv) The effect of non-metal elements on the growth of CNTs needs to be deeply researched. (v) The approach of growing CNTs by calcination is too monotonous, thus we need to further develop various energy supply methods. Therefore, in future research work, we will overcome the practical obstacles by designing precise experiments and specific MOF structures, so as to obtain more controllable and diverse MOF-derived CNT-based composite materials for practical applications.

Conflicts of interest

There are no conflicts to declare.

Acknowledgements

This work was financially supported by the National Natural Science Foundation of China (51972237, 51920105004, 51672193, 51420105002), and also funded by the State Key Laboratory of Structural Chemistry, Chinese Academy of Sciences (20190008). We also acknowledge financial support from the Excellent Youth Cultivation Project of Wenzhou University.

Notes and references

1 A. Magrez, R. Smajda, J. W. Seo, E. Horváth, P. R. Ribic, J. C. Andresen, D. Acquaviva, A. Olariu, G. Laurenczy and L. Forró, *ACS Nano*, 2011, **5**, 3428–3437.
2 L. V. Radushkevich and V. M. Lukyanovich, *Zh. Fiz. Khim.*, 1952, **26**, 88–95.
3 S. Iijima, *Nature*, 1991, **354**, 56–58.
4 J. Prasek, J. Drbohlavova, J. Chomoucka, J. Hubalek, O. Jasek, V. Adam and R. Kizek, *J. Mater. Chem.*, 2011, **21**, 15872.
5 M. S. Dresselhaus, G. Dresselhaus and R. Saito, *Carbon*, 1995, **33**, 883–891.
6 A. Qiu and D. F. Bahr, *Carbon*, 2013, **55**, 335–342.
7 R. Zhang, Q. Wen, W. Qian, D. S. Su, Q. Zhang and F. Wei, *Adv. Mater.*, 2011, **23**, 3387–3391.
8 P. C. Sun, Y. L. Wu, J. W. Gao, G. A. Cheng, G. Chen and R. T. Zheng, *Adv. Mater.*, 2013, **25**, 4938–4943.
9 A. Javey, J. Guo, D. B. Farmer, Q. Wang, D. Wang, R. G. Gordon, M. Lundstrom and H. Dai, *Nano Lett.*, 2004, **4**, 447–450.
10 A. Mikhalchan, A. M. Banas, K. Banas, A. M. Borkowska, M. Nowakowski, M. B. H. Breese, W. M. Kwiatek, C. Paluszkiewicz and T. E. Tay, *Chem. Mater.*, 2018, **30**, 1856–1864.
11 R. Zhang, Y. Zhang, Q. Zhang, H. Xie, H. Wang, J. Nie, Q. Wen and F. Wei, *Nat. Commun.*, 2013, **4**, 1727.
12 M. Jian, H. Xie, Q. Wang, K. Xia, Z. Yin, M. Zhang, N. Deng, L. Wang, T. Ren and Y. Zhang, *Nanoscale*, 2016, **8**, 13437–13444.
13 R. Zhang, Y. Zhang and F. Wei, *Chem. Soc. Rev.*, 2017, **46**, 3661–3715.
14 Y. Li, M. Gong, Y. Liang, J. Feng, J.-E. Kim, H. Wang, G. Hong, B. Zhang and H. Dai, *Nat. Commun.*, 2013, **4**, 1805.
15 Y. J. Sa, D.-J. Seo, J. Woo, J. T. Lim, J. Y. Cheon, S. Y. Yang, J. M. Lee, D. Kang, T. J. Shin, H. S. Shin, H. Y. Jeong, C. S. Kim, M. G. Kim, T.-Y. Kim and S. H. Joo, *J. Am. Chem. Soc.*, 2016, **138**, 15046–15056.
16 S. H. Jin, S. N. Dunham, J. Song, X. Xie, J. H. Kim, C. Lu, A. Islam, F. Du, J. Kim, J. Felts, Y. Li, F. Xiong, M. A. Wahab, M. Menon, E. Cho, K. L. Grosse, D. J. Lee, H. U. Chung, E. Pop, M. A. Alam, W. P. King, Y. Huang and J. A. Rogers, *Nat. Nanotechnol.*, 2013, **8**, 347–355.
17 Y. Wang, D. Liu, H. Zhang, J. Wang, R. Du, T. T. Li, J. Qian, Y. Hu and S. Huang, *Nano Lett.*, 2020, **20**, 496–501.
18 M. Fujii, X. Zhang, H. Xie, H. Ago, K. Takahashi, T. Ikuta, H. Abe and T. Shimizu, *Phys. Rev. Lett.*, 2005, **95**, 065502.
19 R. J. Sager, P. J. Klein, D. C. Lagoudas, Q. Zhang, J. Liu, L. Dai and J. W. Baur, *Compos. Sci. Technol.*, 2009, **69**, 898–904.
20 K. A. Shah and B. A. Tali, *Mater. Sci. Semicond. Process.*, 2016, **41**, 67–82.
21 C. Liu and H.-M. Cheng, *Mater. Today*, 2013, **16**, 19–28.
22 H. Li, M. Eddaoudi, M. O'Keeffe and O. M. Yaghi, *Nature*, 1999, **402**, 276.
23 F. Ran, X. Xu, D. Pan, Y. Liu, Y. Bai and L. Shao, *Nano-Micro Lett.*, 2020, **12**, 46.
24 X. Q. Li, C. L. Hao, B. C. Tang, Y. Wang, M. Liu, Y. W. Wang, Y. H. Zhu, C. G. Lu and Z. Y. Tang, *Nanoscale*, 2017, **9**, 2178–2187.
25 X. Wang, Z. Ma, L. Chai, L. Xu, Z. Zhu, Y. Hu, J. Qian and S. Huang, *Carbon*, 2019, **141**, 643–651.
26 Q. Li, J. Wu, L. Huang, J. Gao, H. Zhou, Y. Shi, Q. Pan, G. Zhang, Y. Du and W. Liang, *J. Mater. Chem. A*, 2018, **6**, 12115–12124.
27 A. Aijaz, J. Masa, C. Rosler, W. Xia, P. Weide, A. J. Botz, R. A. Fischer, W. Schuhmann and M. Muhler, *Angew. Chem., Int. Ed.*, 2016, **55**, 4087–4091.
28 G. Wang, S. Oswald, M. Loffler, K. Mullen and X. Feng, *Adv. Mater.*, 2019, **31**, 1807712.
29 H. Gao, Y. Hu, Y. Xuan, J. Li, Y. Yang, R. V. Martinez, C. Li, J. Luo, M. Qi and G. J. Cheng, *Science*, 2014, **346**, 1352–1356.
30 L. Chong, J. Wen, J. Kubal, F. G. Sen, J. Zou, J. Greeley, M. Chan, H. Barkholtz, W. Ding and D.-J. Liu, *Science*, 2018, **362**, 1276.
31 X. Wang, L. Chai, J. Ding, L. Zhong, Y. Du, T.-T. Li, Y. Hu, J. Qian and S. Huang, *Nano Energy*, 2019, **62**, 745.
32 P. Pachfule, D. Shinde, M. Majumder and Q. Xu, *Nat. Chem.*, 2016, **8**, 718–724.
33 X. Wang, Z. Zhu, L. Chai, J. Ding, L. Zhong, A. Dong, T.-T. Li, Y. Hu, J. Qian and S. Huang, *J. Power Sources*, 2019, **440**, 227158.
34 Y. Ma, Y. Ma, D. Bresser, Y. Ji, D. Geiger, U. Kaiser, C. Streb, A. Varzi and S. Passerini, *ACS Nano*, 2018, **12**, 7220–7231.
35 K. Y. Zou, Y. C. Liu, Y. F. Jiang, C. Y. Yu, M. L. Yue and Z. X. Li, *Inorg. Chem.*, 2017, **56**, 6184–6196.
36 R. Wang, X. Y. Dong, J. Du, J. Y. Zhao and S. Q. Zang, *Adv. Mater.*, 2018, **30**, 1703711.
37 L. Yang, X. Zeng, D. Wang and D. Cao, *Energy Storage Mater.*, 2018, **12**, 277–283.
38 P. Su, H. Xiao, J. Zhao, Y. Yao, Z. Shao, C. Li and Q. Yang, *Chem. Sci.*, 2013, **4**, 2941.
39 Y. Wu, X. Qiu, F. Liang, Q. Zhang, A. Koo, Y. Dai, Y. Lei and X. Sun, *Appl. Catal., B*, 2019, **241**, 407–414.
40 Y. Pan, K. Sun, S. Liu, X. Cao, K. Wu, W. C. Cheong, Z. Chen, Y. Wang, Y. Li, Y. Liu, D. Wang, Q. Peng, C. Chen and Y. Li, *J. Am. Chem. Soc.*, 2018, **140**, 2610–2618.
41 Q. Liang, Z. Chen, X. Chen and Y. Li, *J. Mater. Chem. A*, 2019, **7**, 20310–20316.
42 H. Jin, H. Zhou, D. He, Z. Wang, Q. Wu, Q. Liang, S. Liu and S. Mu, *Appl. Catal., B*, 2019, **250**, 143–149.
43 H. Jin, H. Zhou, W. Li, Z. Wang, J. Yang, Y. Xiong, D. He, L. Chen and S. Mu, *J. Mater. Chem. A*, 2018, **6**, 20093–20099.
44 Z. Zhang, H. Jin, J. Zhu, W. Li, C. Zhang, J. Zhao, F. Luo, Z. Sun and S. Mu, *Carbon*, 2020, **161**, 502–509.
45 T. Liu, P. Zhao, X. Hua, W. Luo, S. Chen and G. Cheng, *J. Mater. Chem. A*, 2016, **4**, 11357–11364.
46 S. Zhang, Q. Wu, L. Tang, Y. Hu, M. Wang, J. Zhao, M. Li, J. Han, X. Liu and H. Wang, *ACS Appl. Mater. Interfaces*, 2018, **10**, 39757–39767.
47 J. Meng, C. Niu, L. Xu, J. Li, X. Liu, X. Wang, Y. Wu, X. Xu, W. Chen, Q. Li, Z. Zhu, D. Zhao and L. Mai, *J. Am. Chem. Soc.*, 2017, **139**, 8212–8221.
48 M. Sindoro, N. Yanai, A. Y. Jee and S. Granick, *Acc. Chem. Res.*, 2014, **47**, 459–469.
49 W. Liu, J. Huang, Q. Yang, S. Wang, X. Sun, W. Zhang, J. Liu and F. Huo, *Angew. Chem., Int. Ed.*, 2017, **56**, 5512–5516.

50 P. Zuo, H. Zhang, M. He, Q. Li, Y. Ma, C. Du, X. Cheng, H. Huo, Y. Gao and G. Yin, *Carbon*, 2017, **122**, 635–642.
51 L. Liu, Y. Wang, F. Yan, C. Zhu, B. Geng, Y. Chen and S. l. Chou, *Small Methods*, 2020, **4**, 1900571.
52 G. N. Ayre, T. Uchino, B. Mazumder, A. L. Hector, J. L. Hutchison, D. C. Smith, P. Ashburn and C. H. de Groot, *J. Phys.: Condens. Matter*, 2011, **23**, 394201.
53 Y. Li, R. Cui, L. Ding, Y. Liu, W. Zhou, Y. Zhang, Z. Jin, F. Peng and J. Liu, *Adv. Mater.*, 2010, **22**, 1508–1515.
54 M. Kusunoki, M. Rokkaku and T. Suzuki, *Appl. Phys. Lett.*, 1997, **71**, 2620–2622.
55 R. L. Van der Wal and L. J. Hall, *Chem. Phys. Lett.*, 2001, **349**, 178–184.
56 J. Gavillet, A. Loiseau, C. Journet, F. Willaime, F. Ducastelle and J. C. Charlier, *Phys. Rev. Lett.*, 2001, **87**, 275504.
57 C. Emmenegger, J. M. Bonard, P. Mauron, P. Sudan, A. Lepora, B. Grobety, A. Züttel and L. Schlapbach, *Carbon*, 2003, **41**, 539–547.
58 Z. Liang, X. Fan, H. Lei, J. Qi, Y. Li, J. Gao, M. Huo, H. Yuan, W. Zhang, H. Lin, H. Zheng and R. Cao, *Angew. Chem., Int. Ed.*, 2018, **57**, 1–6.
59 J.-M. Aguiar-Hualde, Y. Magnin, H. Amara and C. Bichara, *Carbon*, 2017, **120**, 226–232.
60 J.-T. Ren, L. Chen, Y.-S. Wang, W.-W. Tian, L.-J. Gao and Z.-Y. Yuan, *ACS Sustainable Chem. Eng.*, 2020, **8**, 223–237.
61 X. Zhang, X. Zhang, H. Yuan, K. Li, Q. Ouyang, C. Zhu, S. Zhang and Y. Chen, *Chem. Eng. J.*, 2020, **383**, 123208.
62 Z. Li, L. Cai, M. Song, Y. Shen, X. Wang, J. Li, J. Wang, P. Wang and L. Tian, *Electrochim. Acta*, 2020, **339**, 135886.
63 G. Cheng, I. Calizo and A. R. Hight Walker, *Carbon*, 2015, **81**, 678–687.
64 M. Kosaka, S. Takano, K. Hasegawa and S. Noda, *Carbon*, 2015, **82**, 254–263.
65 S. A. Steiner, T. F. Baumann, B. C. Bayer, R. Blume, M. A. Worsley, W. J. MoberlyChan, E. L. Shaw, R. Schlögl, A. J. Hart, S. Hofmann and B. L. Wardle, *J.Am. Chem. Soc.*, 2009, **131**, 12144–12154.
66 A. Kudo, S. A. Steiner, B. C. Bayer, P. R. Kidambi, S. Hofmann, M. S. Strano and B. L. Wardle, *J. Appl. Phys.*, 2017, **122**, 014301.
67 P. R. Kidambi, B. C. Bayer, R. S. Weatherup, R. Ochs, C. Ducati, D. V. Szabó and S. Hofmann, *Phys. Status Solidi RRL*, 2011, **5**, 341–343.
68 J. Kim, C. Young, J. Lee, M. S. Park, M. Shahabuddin, Y. Yamauchi and J. H. Kim, *Chem. Commun.*, 2016, **52**, 13016–13019.
69 R. Wang, T. Yan, L. Han, G. Chen, H. Li, J. Zhang, L. Shi and D. Zhang, *J. Mater. Chem. A*, 2018, **6**, 5752–5761.
70 M. Stadermann, S. P. Sherlock, J.-B. In, F. Fornasiero, H. G. Park, A. B. Artyukhin, Y. Wang, J. J. De Yoreo, C. P. Grigoropoulos, O. Bakajin, A. A. Chernov and A. Noy, *Nano Lett.*, 2009, **9**, 738–744.
71 X. Chen, J. Gao, S. Liu, Z. Yang, S. Wang, Z. Su, P. Zhu, X. Zhao and G. Wang, *J. Alloys Compd.*, 2020, **828**, 154435.
72 H. Zhou, D. He, A. I. Saana, J. Yang, Z. Wang, J. Zhang, Q. Liang, S. Yuan, J. Zhu and S. Mu, *Nanoscale*, 2018, **10**, 6147–6154.
73 L. Wang, Y. Jiao, S. Yao, P. Li, R. Wang and G. Chen, *Inorg. Chem. Front.*, 2019, **6**, 1553–1560.
74 C. Yang, M. Zhou, C. He, Y. Gao, S. Li, X. Fan, Y. Lin, F. Cheng, P. Zhu and C. Cheng, *Nano-Micro Lett.*, 2019, **11**, 87.
75 X. Zhao, P. Pachfule, S. Li, J. R. J. Simke, J. Schmidt and A. Thomas, *Angew. Chem., Int. Ed.*, 2018, **57**, 8921–8926.
76 J. Wang, W. Liu, G. Luo, Z. Li, C. Zhao, H. Zhang, M. Zhu, Q. Xu, X. Wang, C. Zhao, Y. Qu, Z. Yang, T. Yao, Y. Li, Y. Lin, Y. Wu and Y. Li, *Energy Environ. Sci.*, 2018, **11**, 3375–3379.
77 S. Hanif, N. Iqbal, X. Shi, T. Noor, G. Ali and A. M. Kannan, *Renewable Energy*, 2020, **154**, 508–516.
78 Z. Dong, G. Liu, S. Zhou, Y. Zhang, W. Zhang, A. Fan, X. Zhang and X. Dai, *ChemCatChem*, 2018, **10**, 5475–5486.
79 W. Zhou, Z. Han, J. Wang, Y. Zhang, Z. Jin, X. Sun, Y. Zhang, C. Yan and Y. Li, *Nano Lett.*, 2006, **6**, 2987–2990.
80 D. Takagi, Y. Kobayashi, H. Hibino, S. Suzuki and Y. Homma, *Nano Lett.*, 2008, **8**, 832–835.
81 X. Shi, H. Yang, P. Sun, G. Shao, X. Duan and X. Zhen, *Carbon*, 2007, **45**, 1735–1742.
82 M. Masteri-Farahani and S. Abednatanzi, *Inorg. Chem. Commun.*, 2013, **37**, 39–42.
83 L. Qiu and F. Ding, *Phys. Rev. Lett.*, 2019, **123**, 256101.
84 X. Zheng, J. Deng, N. Wang, D. Deng, W. H. Zhang, X. Bao and C. Li, *Angew. Chem., Int. Ed.*, 2014, **53**, 7023–7027.
85 Y. Pang, S. Chen, C. Xiao, S. Ma and S. Ding, *J. Mater. Chem. A*, 2019, **7**, 4126–4133.
86 J. S. Li, S. L. Li, Y. J. Tang, M. Han, Z. H. Dai, J. C. Bao and Y. Q. Lan, *Chem. Commun.*, 2015, **51**, 2710–2713.
87 X. Jin, J. Lim, Y. Ha, N. H. Kwon, H. Shin, I. Y. Kim, N.-S. Lee, M. H. Kim, H. Kim and S.-J. Hwang, *Nanoscale*, 2017, **9**, 12416–12424.
88 Y. Wang, J. Ma, J. Wang, S. Chen, H. Wang and J. Zhang, *Adv. Energy Mater.*, 2019, **9**, 1802939.
89 R. Wu, D. P. Wang, V. Kumar, K. Zhou, A. W. K. Law, P. S. Lee, J. Lou and Z. Chen, *Chem. Commun.*, 2015, **51**, 3109–3112.
90 Y. Fang, X. Y. Yu and X. W. D. Lou, *Adv. Mater.*, 2018, **30**, 1706668.
91 K. Guo, B. Xi, R. Wei, H. Li, J. Feng and S. Xiong, *Adv. Energy Mater.*, 2020, **10**, 1902913.
92 X. Wang, H. Yin, G. Sheng, W. Wang, X. Zhang and Z. Lai, *ACS Appl. Nano Mater.*, 2018, **1**, 7075–7082.
93 Y. Xu, P. Deng, G. Chen, J. Chen, Y. Yan, K. Qi, H. Liu and B. Y. Xia, *Adv. Funct. Mater.*, 2020, **30**, 1906081.
94 W. Miao, Y. Zhang, H. Li, Z. Zhang, L. Li, Z. Yu and W. Zhang, *J. Mater. Chem. A*, 2019, **7**, 5504–5512.
95 T. Liu, L. Zhang and Y. Tian, *J. Mater. Chem. A*, 2018, **6**, 5935–5943.
96 A. Aijaz, J. Masa, C. Rosler, H. Antoni, R. A. Fischer, W. Schuhmann and M. Muhler, *Chem. – Eur. J.*, 2017, **23**, 12125–12130.
97 X. Xu, F. Ran, Z. Fan, H. Lai, Z. Cheng, T. Lv, L. Shao and Y. Liu, *ACS Appl. Mater. Interfaces*, 2019, **11**, 13564–13573.
98 C. Zhao, X. Dai, T. Yao, W. Chen, X. Wang, J. Wang, J. Yang, S. Wei, Y. Wu and Y. Li, *J. Am. Chem. Soc.*, 2017, **139**, 8078–8081.
99 K. Zhang, Y. Zhang, Q. Zhang, Z. Liang, L. Gu, W. Guo, B. Zhu, S. Guo and R. Zou, *Carbon Energy*, 2020, **2**, 283–293.
100 D. Das, S. Santra and K. K. Nanda, *ACS Appl. Mater. Interfaces*, 2018, **10**, 35025–35038.
101 B. Y. Xia, Y. Yan, N. Li, H. B. Wu, X. W. Lou and X. Wang, *Nat. Energy*, 2016, **1**, 15006.
102 Z. Chen, R. Wu, Y. Liu, Y. Ha, Y. Guo, D. Sun, M. Liu and F. Fang, *Adv. Mater.*, 2018, **30**, 1802011.
103 D. Ji, L. Fan, L. Li, N. Mao, X. Qin, S. Peng and S. Ramakrishna, *Carbon*, 2019, **142**, 379–387.
104 Z. Zhao, C. Gao, K. Ma and Y. Lu, *Appl. Surf. Sci.*, 2020, **504**, 144380.
105 S. M. Unni, G. M. Anilkumar, M. Matsumoto, T. Tamaki, H. Imai and T. Yamaguchi, *Sustainable Energy Fuels*, 2017, **1**, 1524–1532.
106 W. Li, W. Ding, Y. Nie, Q. He, J. Jiang and Z. Wei, *ACS Appl. Mater. Interfaces*, 2019, **11**, 22290–22296.
107 C. Jin, K. Suenaga and S. Iijima, *ACS Nano*, 2008, **2**, 1275–1279.
108 M. Yudasaka, R. Kikuchi, Y. Ohki and S. Yoshimura, *Carbon*, 1997, **35**, 195–201.
109 L. Chai, L. Zhang, X. Wang, Z. Ma, T.-T. Li, H. Li, Y. Hu, J. Qian and S. Huang, *Electrochim. Acta*, 2019, **321**, 134680.
110 M. Müller, O. I. Lebedev and R. A. Fischer, *J. Mater. Chem.*, 2008, **18**, 5274–5281.
111 S. Wang, J. Qin, T. Meng and M. Cao, *Nano Energy*, 2017, **39**, 626–638.
112 G. Jia, W. Zhang, G. Fan, Z. Li, D. Fu, W. Hao, C. Yuan and Z. Zou, *Angew. Chem., Int. Ed.*, 2017, **56**, 13781–13785.
113 L. Zou, C. C. Hou, Z. Liu, H. Pang and Q. Xu, *J. Am. Chem. Soc.*, 2018, **140**, 15393–15401.
114 Q. Yuan, Y. Yu, Y. Gong and X. Bi, *ACS Appl. Mater. Interfaces*, 2020, **12**, 3592–3602.
115 L. Chai, Z. Hu, X. Wang, Y. Xu, L. Zhang, T. T. Li, Y. Hu, J. Qian and S. Huang, *Adv. Sci.*, 2020, **7**, 1903195.
116 L. Xu, X. Wang, L. Chai, T.-T. Li, Y. Hu, J. Qian and S. Huang, *Mater. Lett.*, 2019, **248**, 181–184.
117 L. Yang, Y. Lv and D. Cao, *J. Mater. Chem. A*, 2018, **6**, 3926–3932.
118 S. Su, Y. Wang, J. Qin, C. Wang, Z. Yao, R. Lu and Q. Wang, *J. Mater. Sci.*, 2019, **54**, 12498–12508.
119 P. R. Bandaru, C. Daraio, K. Yang and A. M. Rao, *J. Appl. Phys.*, 2007, **101**, 094307.
120 Z. Yang, C. Zhao, Y. Qu, H. Zhou, F. Zhou, J. Wang, Y. Wu and Y. Li, *Adv. Mater.*, 2019, **31**, 1808043.
121 A. Indra, U. Paik and T. Song, *Angew. Chem., Int. Ed.*, 2018, **57**, 1241–1245.

122 M. Du, D. Song, A. Huang, R. Chen, D. Jin, K. Rui, C. Zhang, J. Zhu and W. Huang, *Angew. Chem., Int. Ed.*, 2019, **58**, 5307–5311.
123 H. Sun, Y. Lian, C. Yang, L. Xiong, P. Qi, Q. Mu, X. Zhao, J. Guo, Z. Deng and Y. Peng, *Energy Environ. Sci.*, 2018, **11**, 2363–2371.
124 M. Yang, Y. Yuan, Y. Li, X. Sun, S. Wang, L. Liang, Y. Ning, J. Li, W. Yin, R. Che and Y. Li, *Carbon*, 2020, **161**, 517–527.
125 H. Furukawa, K. E. Cordova, M. O'Keeffe and O. M. Yaghi, *Science*, 2013, **341**, 1230444.
126 Z. Wang, J. Ang, B. Zhang, Y. Zhang, X. Y. D. Ma, T. Yan, J. Liu, B. Che, Y. Huang and X. Lu, *Appl. Catal., B*, 2019, **254**, 26–36.
127 L. Zhang, X. Wang, R. Wang and M. Hong, *Chem. Mater.*, 2015, **27**, 7610–7618.